High-quality and highly-transparent AlN template on annealed sputter-deposited AlN buffer layer for deep ultra-violet light-emitting diodes

Chia-Yen Huang, Pei-Yu Wu, Kai-Shiang Chang, Yun-Hsiang Lin, Wei-Chih Peng, Yem-Yeu Chang, Jui-Ping Li, Hung-Wei Yen, YewChung Sermon Wu, Hideto Miyake, and Hao-Chung Kuo

Citation: AIP Advances **7**, 055110 (2017); doi: 10.1063/1.4983708

View online: http://dx.doi.org/10.1063/1.4983708

View Table of Contents: http://aip.scitation.org/toc/adv/7/5

Published by the American Institute of Physics

Articles you may be interested in

150 mW deep-ultraviolet light-emitting diodes with large-area AlN nanophotonic light-extraction structure emitting at 265 nm
Applied Physics Letters **110**, 141106 (2017); 10.1063/1.4978855

Improved performance of AlGaN-based deep ultraviolet light-emitting diodes with nano-patterned AlN/sapphire substrates
Applied Physics Letters **110**, 191103 (2017); 10.1063/1.4983283

III-Nitride-on-silicon microdisk lasers from the blue to the deep ultra-violet
Applied Physics Letters **109**, 231101 (2016); 10.1063/1.4971357

Investigation of the light-extraction efficiency in 280 nm AlGaN-based light-emitting diodes having a highly transparent p-AlGaN layer
Journal of Applied Physics **121**, 013105 (2017); 10.1063/1.4973493

HAVE YOU HEARD?
Employers hiring scientists and engineers trust
PHYSICS TODAY | JOBS
www.physicstoday.org/jobs

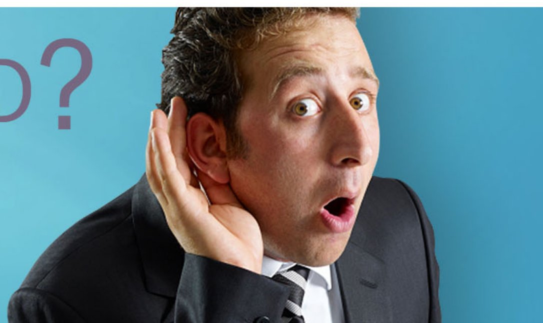

High-quality and highly-transparent AlN template on annealed sputter-deposited AlN buffer layer for deep ultra-violet light-emitting diodes

Chia-Yen Huang,[1,a] Pei-Yu Wu,[2] Kai-Shiang Chang,[1] Yun-Hsiang Lin,[3] Wei-Chih Peng,[3] Yem-Yeu Chang,[4] Jui-Ping Li,[4] Hung-Wei Yen,[5] YewChung Sermon Wu,[2] Hideto Miyake,[6] and Hao-Chung Kuo[1]

[1]*Department of Photonics and Institute of Electro-Optical Engineering, National Chiao Tung University, 1001 Ta Hsueh Rd., Hsinchu 300, Taiwan*
[2]*Department of Materials Science and Engineering, National Chiao-Tung University, 1001 Ta Hsueh Rd., Hsinchu 300, Taiwan*
[3]*Research and Development Center, Epistar Corporation, 21, Li-Hsin Rd., Hsinchu Science Park, Hsinchu 300, Taiwan*
[4]*Advanced Technology Development Division, Crystalwise Technology Inc., No.8, Ke Bei 5th Rd., Jhunan Science Park, Miaoli County 35053, Taiwan*
[5]*Department of Materials Science and Engineering, National Chiao-Tung University, No. 1, Sec. 4, Roosevelt Road, 10617 Taipei, Taiwan*
[6]*Department of Electrical and Electronic Engineering, Mie University, 1577 Kurimamachiya, Tsu, Mie 514-8507, Japan*

(Received 9 March 2017; accepted 1 May 2017; published online 15 May 2017)

A high-quality and highly-transparent AlN template was prepared by regrowth on a sputter-deposited AlN buffer layer. The buffer layer was thermally annealed and then underwent AlN regrowth in metalorganic chemical vapor deposition (MOCVD). The peakwidth of (002) and (102) plane x-ray rocking curve was 104 arcsec and 290 arcsec, respectively, indicating a threading dislocation density $<5.0 \times 10^8$ cm^{-2}. Dislocations were reduced via grain growth and morphological evolution. The absence of carbon impurity source in sputter deposition also resulted in an improved transparency. According to transmission and reflection measurements, the absorption rate of λ=280 nm emission propagating through the template was less than 6%. *© 2017 Author(s). All article content, except where otherwise noted, is licensed under a Creative Commons Attribution (CC BY) license (http://creativecommons.org/licenses/by/4.0/).* [http://dx.doi.org/10.1063/1.4983708]

INTRODUCTION

Nitride-based deep ultra-violet (λ= 270 nm~280 nm) light-emitting diodes (LED) have caught much attention in the past few years for their potential in water purification, sterilization, and other bio-medical applications.[1,2] To date, the performance of deep ultra-violet (UV) LEDs is still quite limited due to many technical difficulties. The internal quantum efficiency (IQE) suffered from high threading dislocation densities (TDD) originating from the AlN template. High-quality AlN templates have been grown on bulk single crystal AlN substrates with TDD$<10^8$ cm^{-2}.[3–5] High-quality AlN epitaxy could be obtained with less difficulties by homoepitaxy because of their zero lattice mismatch. However, the long absorption path in the bulk AlN substrates with UV-active impurity levels imposed a strong challenge in overall light-extraction efficiency of deep-UV LEDs,[6,7] especially when the LED structures were often capped with a band-edge absorbing p-GaN layer as the electrical contact. Sapphire, the most commonly used substrates for InGaN-based blue emitters, is a more practical candidate for fabricating AlN template due to its high UV-transparency and wide

[a]Email: yenhuang@nctu.edu.tw

 © Author(s) 2017

commercial availability. TDD of GaN templates on sapphire was reported to be less than 10^8 cm^{-2}.[8] However, the crystal quality of AlN templates on sapphire prepared by similar two-step growth techniques were much poorer. TDD of those AlN template was still in the range of $10^9 \sim 10^{10}$ cm^{-2}.[9,10] The ineffectiveness of TDD reduction during epitaxial growth was attributed to the poor Al adatom mobility. Hirayama et al. and Funato et al. applied a pulsed-flow of ammonia and precursors to promote the coalescence of AlN grains with the cost of overall growth rate.[11,12] Many groups also tried different schemes of growth condition modulation to improve the crystal quality of AlN templates, but the reported FWHM's of (102) rocking curve were still in the levels of 400 arcsec to 600 arcsec.[13,14] Recently, Miyake et al. applied an ex-situ high-temperature annealing (T>1600 °C) on a MOCVD-grown AlN layer on sapphire, which triggered the recrystallization of the buffer layer.[15] After MOCVD regrowth (T_g=1450 °C) under a relatively high temperature, the measured FWHM of (102) plane rocking curves was down to 154 arcsec. In this report, we investigated the TDD evolution during the annealing and the regrowth process using sputter-deposited AlN (sputter-AlN) as the initial buffer layer instead. The benefit of using sputter-AlN buffer over MOCVD-grown buffer will also be discussed.

EXPERIMENTAL

The sample preparation process was schematically illustrated as figure 1. 300 nm thick AlN buffer layer was sputtered on commercial 2-inch single-side polished (0001) sapphire substrates. The offcut of sapphire was 0.2 ∓ 0.05 degree toward $[10\bar{1}0]$ direction (m-axis), which was calibrated by high-resolution x-ray diffractometer (HR-XRD). High purity Al (at%>99.999%) was bombarded by Ar ions and then reacted with N_2 plasma to form AlN film on the substrate surface. The AlN buffer layer was annealed under N_2 ambient with annealing temperature between 1600 °C and 1700 °C to provoke recrystallization in AlN film while preventing surface reconstruction of the sapphire substrate. 2.5 μm AlN was regrown directly on annealed buffer layer by MOCVD without additional in-situ cleaning or nitridation treatment. The growth pressure and temperature was 10 kPa and 1300 °C, respectively. To protect the regrowth surface, TMAl and NH_3 were injected into chamber during the temperature ramping stage. The AlN growth rate was around 3 μm/hr. The surface morphology was characterized by atomic force spectroscopy (AFM) under tapping mode with a resolution of 1024 pixels in each 5 μm long scan. The crystal quality was characterized by Jordan Valley QC3 HR-XRD with asymmetric Ge(220) two-bounce monochromator and a 1 mm × 10 mm slit before detector. Cross-sectional scanning transmission electron microscope (STEM) measurement was conducted in JEOL-JEM-2010F. The TEM sample was cut and lifted by focus ion-beam technique in FEI Helios 1200+ and then attached to copper grid for characterization. The sample cross-section was parallel to $(11\bar{2}0)$ plane with a sample thickness around 100 nm.

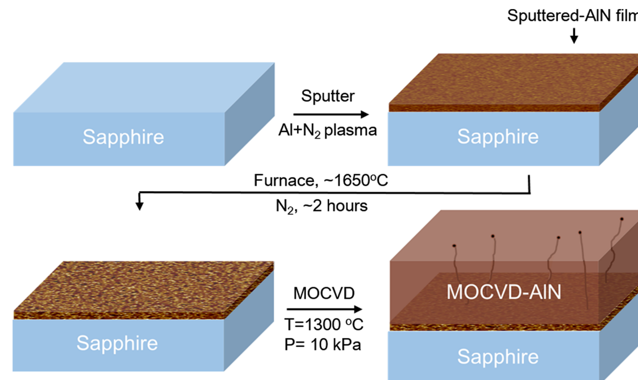

FIG. 1. Schematic fabrication process of AlN template on sapphire with an annealed sputter-deposited AlN buffer layer.

RESULT AND DISCUSSION

The AFM images and x-ray rocking curves of (002) plane and (102) plane under different stages of processing were summarized from figure 2a–figure 2e. The AFM images of the as-deposited film (figure 2a) and the annealed film (figure 2b) both showed a grain-like morphology in the sputtered-AlN layers. The height variation on the surface and grain sizes were slightly enhanced after annealing process. Roughness average (R_a) increased from 0.4 nm to 1.0 nm after annealing. After AlN regrowth in MOCVD, the surface morphology gradually evolve to terrace-like macrosteps with step heights of 6 to 10 Al-N bilayers. The inclination angle of macrostep terraces was estimated to be around 0.16 degree ∼0.18 degree, which is closed to the offcut of the substrates. The FWHM's of (002) rocking curves were much lower than those of (102) rocking curves in all stages. After regrowth, the XRD FWHM of (002) and (102) plane was 104 arcsec and 290 arcsec, respectively. According to the relation between the Burger's vector and XRD Bragg peakwidth broadening, the TDD in AlN layers were dominated by pure-edge type dislocations. To quantify the densities of edge and screw dislocations, coherent length model developed by Lee et al. was adopted:[16]

$$\beta_{hkl}^2 = \beta_{tilt}^2 \cos^2 \chi_{hkl} + \beta_{twist}^2 \cos^2 \chi_{hkl}$$

$$\rho_{screw} = \beta_{tilt}^2 / 4.53 b_c^2$$

$$\rho_{edge} = \beta_{twist}^2 / 4.53 b_a^2$$

where β_{hkl} is the FWHM of (hkl) plane rocking curves, χ_{hkl} is the inclination angle between (hkl) plane and (001) plane, β_{tilt} and β_{twist} is internal material parameters that need to be extracted, ρ_{screw} and ρ_{edge} is the density of screw-type and edge-type threading dislocations. b_c and b_a is the length of the corresponding Burger's vectors, where b_c=0.4982 nm and b_a=0.3112 nm, respectively. The calculated dislocation densities and roughness in each stage were plotted in figure 2f. The

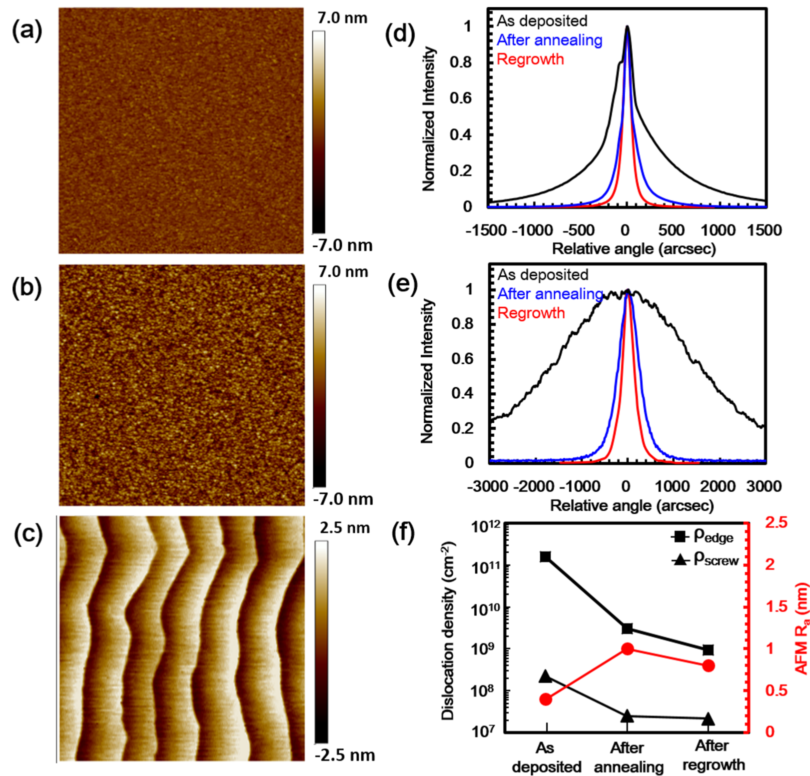

FIG. 2. 5 µm×5 µm AFM image of (a) as-deposited (b) annealed buffer layer and (c) template after regrowth. (d) (002) plane (e) (102) plane x-ray rocking curves in each stage. (f) Evaluated densities of edge dislocation (black square), screw dislocation (black triangle) and roughness average (red circle) in each stage.

TDD of edge dislocation (ρ_{edge}~1.59×10^{11} cm^{-2}) is three-order higher than that of screw dislocations (ρ_{screw}~2.22×10^{8} cm^{-2}), which is attributed to the high density of twisted grain boundaries in the sputtered AlN film.[16] After annealing, the TDD of screw-type and edge-type dislocations was only 11.2% and 1.9% of its original values. The drastic reduction of ρ_{edge} was driven by lowering total energy of twisted grain boundaries. Normal grain growth nucleated in the sputter AlN layer. Although the columnar microstructure within buffer layer was mostly eliminated, the trace of grain-like morphology was retained due to a limited atomic migration on the surface. In comparison, Miyake et al.'s work showed a terrace-like surface morphology after annealing on wither MOCVD-grown or sputtered AlN buffer layers.[15,17] The discrepancy might be attributed to some unraveled difference in processing conditions, leading to the different paths of microstructure evolution. Fortunately, terrace-like morphology can still be achieved after MOCVD regrowth. According to the model, ρ_{screw} and ρ_{edge} after regrowth dropped to 2.20×10^{7} cm^{-2} and 9.51×10^{8} cm^{-2}, respectively. Empirically, this classic model overestimated the actual density of edge dislocation by a factor of 2 to 5.[18,19] Therefore, the actual dislocation density was estimated to be between 2.0×10^{8} cm^{-2} to 5.0×10^{8} cm^{-2}.

Figure 3a showed the cross-sectional bright-field STEM image of the AlN template after regrowth. Because the columnar micro-structure were eliminated after annealing, there is no clear interface between sputtered buffer layer and MOCVD regrown layer. However, the dislocations showed distinct behaviors between the top part and the bottom part of the template. Dislocations at the top were straight and had small inclination angles to the growth normal, while dislocations at the bottom were more curved or more inclined. Figure 3b is a STEM image with larger magnification near the bottom. Abrupt dislocation kinks and dislocation half loops were observed and highlighted in the figure. At the initial stage of the regrowth, the surface gradually evolved from grain-like morphology to macrostep terrace-like morphology. As the macrostep swept through a treading dislocation on a grain-like surface, dislocations were bent and pair annihilation was induced via forming half-loops.[20] After the surface was fully dominated by terrace morphology, the driving mechanism of dislocation bending also diminished. In this stage, the dislocations propagated with growth direction without much inclination. In the other words, reduction of TDD became ineffective after the growth mode stabilized. In this study, the FWHM of (102) plane rocking curve became insensitive to total thickness after its thickness exceeded 2 μm. Therefore, the buffer quality after annealing was critical to the final template quality.

To compare the performance of AlN template in this work with conventional ones, a MOCVD-grown AlN template was prepared by common two-step growth techniques as a reference. Low-temperature AlN (LT-AlN) buffer layer was grown in MOCVD under T= 900 °C and P=10 kPa followed by a high-temperature AlN (HT-AlN) growth with the same condition described in figure 1. After some optimization in buffer growth and pre-growth treatments, the FWHM of (002) plane and (102) plane rocking curves reached the level of 120 arcsec and 480 arcsec, respectively. For brevity, the template with annealed sputter-AlN buffer was named as "sample A" and the one with MOCVD LT-AlN buffer was named as "sample B". Two buffer layer sample, sample C and sample D, were

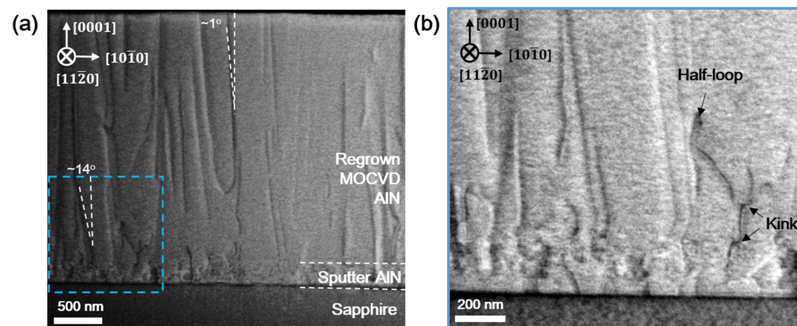

FIG. 3. (a) Cross-sectional STEM bright-field image of AlN template. Dashed white lines indicated the inclination angle between growth normal and dislocation lines. (b) The magnified image of the area highlighted by light-blue dashed-lines in figure 3(a).

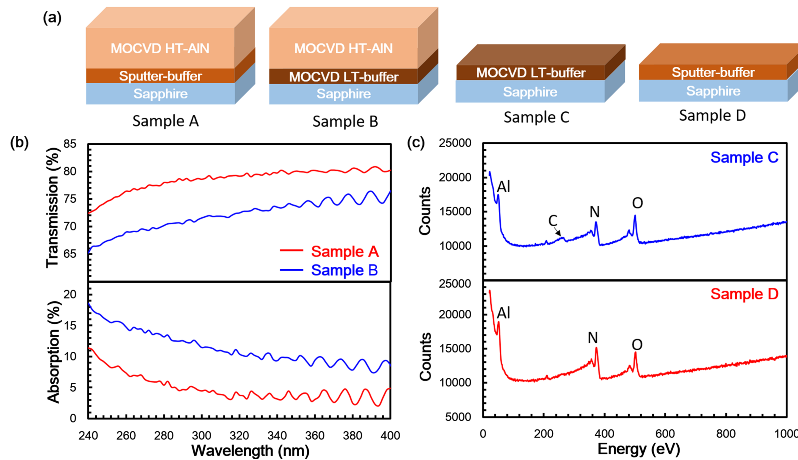

FIG. 4. (a) Schematic structure illustration of different AlN templates (Sample A and B) and buffer layers. (Sample C and D) (b)The transmission and absorption spectrum of sample A and sample B in ultraviolet region. (c) Auger electron spectroscopy results of sample C and sample D.

also prepared for Auger electrons spectroscopy (AES) measurement. Sample C was an interrupted growth of sample B before the HT-AlN growth and sample D was an annealed 300 nm sputter-AlN layer. The structures of sample A to sample D were illustrated in figure 4a. The backside of sample A and sample B were backside-polished for transmission and reflection measurements in Hitachi U-4100 spectrophotometer. Absorption rates were evaluated by subtracting measured transmission rate and reflection rate from unity.

The transmission rate and absorption rate in ultra-violet spectral region from 240 nm to 400 nm was plotted in figure 4b. The absorption rate of sample A was 4% to 8% lower than that of sample B. Since the growth condition of high-temperature AlN was the same, the excessive light absorption in sample B was mostly attributed to the buffer layers. In the AES results of sample C and sample D in figure 4c, both samples showed a characteristic energy peak of oxygen (502 eV), which is difficult to avoid on a non-passivated Al-containing surface. It's worth noticing that characteristic energy peak of carbon (272 eV) was only observed in sample C. Assuming a 0.1 at% detection limit of AES, the carbon impurity level of sample C was higher than 5×10^{19} cm^{-3}. The high concentration of carbon impurity was attributed to the incomplete pyrolysis of trimethylaluminium (TMAl) precursor under a low-temperature growth. The carbon impurity level of sputtered AlN was inherently low because of the absence of impurity source in the process. According to an investigation from Collazo et al., although the absorption spectrum of carbon impurities peaks around 265 nm, its tail in long wavelength region was also non-negligible when the concentration was high.[21] If we take a closer look in figure 4b, the absorption rate of sample A was around 3% for $\lambda>310$ nm and it rose when the wavelength became shorter than that. This was attributed to the onset activation of $(V_{Al} - O_N)^{2-}$ complexes in the HT-AlN.[22,23] For sample B, the absorption rate started to rise from the visible region toward the UV region. In the common emission wavelength of deep-UV LEDs (λ= 270 nm~280 nm), 6% of light was absorbed in sample A and 14% of light was absorbed in sample B. We can tell that LT-AlN buffer contributed the light absorption more than the HT-AlN. The carbon impurity of MOCVD-buffer might be reduced by raising its growth temperature of buffer layer. However, the crystal quality of the whole template will be jeopardized. One might also anneal a MOCVD-grown buffer which was prepared under a high growth temperature to achieve both superior crystal quality and high deep-UV transparency. Under this circumstance, the major issue become the cost-effectiveness competition between these two approaches, which might not have a definite answer. In general, the cost of sputtering is lower than that of MOCVD due to its lower processing temperature and less sophisticated tool design.

In conclusion, we demonstrated a high-quality and a highly-transparent AlN template on sapphire. The dislocations were firstly reduced by coalescence of twisted grains in the annealing process, and further annihilated by the dislocation bending during morphological evolution in the regrowth

process. The TDD of the AlN template has reached ~10^8 cm^{-3} level with only 6% deep-UV absorption rate in a 2 μm-thick AlN template. We believe this approach will be a suitable platform for future development of high-performance deep-UV LEDs.

[1] A. Khan, K. Balakrishnan, and T. Katona, Nat. Photon. **2**, 77 (2008).
[2] H. Hirayama, N. Maeda, S. Fujikawa, S. Toyoda, and N. Kamata, Jpn. J. Appl. Phys. **53**, 100209 (2014).
[3] Z. Ren, Q. Sun, S.-Y. Kwon, J. Han, K. Davitt, Y. K. Song, A. V. Nurmikko, W. Liu, J. Smart, and L. Schowalter, Phys. Stat. Sol. (c) **4**(7), 2482 (2007).
[4] H. J. Kim, S. Choi, D. Yoo, J.-H. Ryou, R. S. Dupuis, R. F. Dalmau, P. Lu, and Z. Sitar, Appl. Phys. Lett. **93**, 022103 (2008).
[5] Y. Kumagai, Y. Kubota, T. Nagashima, T. Kinoshita, R. Dalmau, R. Schlesser, B. Moody, J. Xie, H. Murakami, A. Koukitu, and Z. Sitar, Appl. Phys. Express **5**, 055504 (2012).
[6] M. Strassburg, J. Senawiratne, N. Dietz, U. Haboeck, A. Hoffmann, V. Noveski, R. Dalmau, R. Schlesser, and Z. Sitar, J. Appl. Phys. **96**, 5870 (2004).
[7] M. Bickermann, B. M. Epelbaum, O. Filip, P. Heimann, S. Nagata, and A. Winnacker, Phys. Status Solidi (c) **7**(1), 21 (2010).
[8] H. Y. Shin, S. K. Kwon, Y. I. Chang, M. J. Cho, and K. H. Park, J. Cryst. Growth **311**, 4167 (2009).
[9] Y. Chen, H. Song, D. Li, X. Sun, H. Jiang, Z. Li, G. Miao, Z. Zhang, and Y. Zhou, Materials Letters **114**, 26 (2014).
[10] W. Luo, L. Li, Z. Li, Q. Yang, D. Zhang, X. Dong, D. Peng, L. Pan, C. Li, B. Liu, and R. Zhong, J. Alloys Compd. **697**, 262 (2017).
[11] H. Hirayama, S. Fujikawa, N. Noguchi, J. Norimatsu, T. Takano, K. Tsubaki, and N. Kamata, Phys. Status Solidi A **206**, 1176 (2009).
[12] R. G. Banal, M. Funato, and Y. Kawakami, J. Cryst. Growth **311**, 2834 (2009).
[13] N. Okada, N. Kato, S. Sato, T. Sumii, T. Nagai, N. Fujimoto, M. Imura, K. Balakrishnan, M. Iwaya, S. Kamiyama, H. Amano, I. Akasaki, H. Maruyama, T. Takagi, T. Noro, and A. Bandoh, J. Cryst. Growth **298**, 349 (2007).
[14] X. Zhang, F. J. Xu, J. M. Wang, C. G. He, L. S. Zhang, J. Huang, J. P. Cheng, Z. X. Qin, X. L. Yang, N. Tang, X. Q. Wang, and B. Shen, CrystEngComm **17**, 7496 (2015).
[15] H. Miyake, G. Nishio, S. Suzuki, K. Hiramatsu, H. Fukuyama, J. Kaur, and N. Kuwano, Appl. Phys. Express **9**, 025501 (2016).
[16] S. R. Lee, A. M. West, A. A. Allerman, K. E. Waldrip, D. M. Follstaedt, P. P. Provencio, D. D. Koleske, and C. R. Abernathy, Appl. Phys. Lett. **86**, 241904 (2005).
[17] H. Miyake, C. H. Lin, K. Tokoro, and K. Hiramatsu, J. Cryst. Growth **456**, 155 (2016).
[18] V. Kirchner, M. Fehrer, S. Figge, H. Heinke, S. Einfeldt, D. Hommel, H. Selke, and P. L. Ryder, Phys. Status Solidi B **216**, 659 (1999).
[19] R. Chierchia, T. Böttcher, H. Heinke, S. Einfeldt, S. Figge, and D. Hommel, J. Appl. Phys. **93**, 8918 (2003).
[20] J. Bai, M. Dudley, W. H. Sun, H. M. Wang, and M. A. Khan, Appl. Phys. Lett. **88**, 051903 (2006).
[21] R. Collazo, J. Xie, B. E. Gaddy, Z. Bryan, R. Kirste, M. Hoffmann, R. Dalmau, B. Moody, Y. Kumagai, T. Nagashima, Y. Kubota, T. Kinoshitu, A. Koukitu, D. L. Irving, and Z. Sitar, Appl. Phys. Lett. **100**, 191914 (2012).
[22] A. Sedhain, J. Y. Lin, and H. X. Jiang, Appl. Phys. Lett. **100**, 221107 (2012).
[23] Q. Yan, A. Janotti, M. Scheffler, and C. Van de Walle, Appl. Phys. Lett. **105**, 111104 (2014).